# Plastic Hinge Rotation Capacity of Reinforced HPFRCC Beams

**Ali Hemmati**

Ph.D. Candidate, Civil Engineering Faculty, Semnan University, Semnan, Iran,

Email: ahemmati2000@yahoo.com

**Ali Kheyroddin**

Professor, Civil Engineering Faculty, Semnan University, Semnan, Iran,

Email: kheyroddin@semnan.ac.ir

**Mohammad Kazem Sharbatdar**

Assistant Professor, Civil Engineering Faculty, Semnan University, Semnan, Iran,

Email: msharbatdar@semnan.ac.ir

**Abstract:** High Performance Fiber Reinforced Cementitious Composite (HPFRCC) materials exhibit strain hardening behavior under tensile loading. This strain hardening response occurs after first cracking of the material. In this paper, experimental and parametric studies are performed to assess the influence of the compressive strength, loading type and tension reinforcement ratio (ρ) on the ultimate deformation characteristics of reinforced HPFRCC beams. The analytical and numerical results for simply supported beams with different amounts of tension reinforcement ratio under three different loading conditions are presented and compared with each other and also with the experimental data, where available. The plastic hinge rotation capacity is increased as the loading condition is changed from the concentrated load at the middle to the uniform, and it is a maximum for the case of the two-point load. The effect of the loading type on the plastic rotation capacity of the reinforced beams with high amount of ρ is not as significant as that for the lightly reinforced beams. Based on the analytical results obtained using the nonlinear finite element method, new simple equations as function of the tension reinforcement ratio and the loading type are proposed. The analytical results indicate that the proposed equations can be used with sufficient accuracy for analysis of ultimate capacity and the associated deformations of RHPFRCC beams.

**Keywords:** Nonlinear Analysis, Finite Element, Plastic Hinge, Reinforced Concrete, Rotation Capacity

## a. Introduction

HPFRCC is defined as a material with strain hardening response under uni-axial loading. At the first stages, Li and Wu introduced a pseudo-strain-hardening material that used only fine aggregates with reinforcing polyethylene fibers (Li and Wu 1992). In 1996, Naaman and Reinhardt presented and developed a fiber reinforced cementitious material which had a matrix with no coarse aggregates, and regarded as fiber reinforced cement paste or mortar (Naaman and Reinhardt 1996).As it shown in Fig. 1, high tensile ductility with strain hardening response is the most important characteristics of this material which is called as High Performance Fiber Reinforced Cementitious Composite (HPFRCC) compared to normal concrete and fiber reinforced concrete (FRC). In recent years, a new class of HPFRCC has emerged entitled ECC. Engineered Cementitious Composite (ECC) was originally developed at the University of Michigan, with a typical moderate tensile strength of 4-6 MPa and a higher ductility of 3-5% (Fischer et al 2003). After this stage, self-consolidating ECC, high early strength ECC, light weight ECC and green ECC were introduced by different researchers (Kong et al 2003, Wang and Li 2006, Wang and Li 2003, Lepech et al 2007). A summary of major physical properties of ECC is given in Table 1 (Li 2007). Some of the researchers have worked on nonlinear finite element analysis of concrete and HPFRCC sections (Ghobarah and Aly 1998, Shaheen and Shrive 2008, Ranzi and Bradford 2009). Results showed that there is an appropriate compatibility between experimental tests and analytical investigations in regard of concrete and HPFRCC (Han et al 2003, Sirijaroonchai 2009, Na and Kwak 2011).

A large number of researchers have developed ECC material based on PVA fiber. But, decision making on selecting and using the type of fibers, depends on fiber's natural characteristics such as diameter ranges, surface characteristics and mechanical behavior. It also depends on the matrix cracking properties, fiber-matrix interfacial bonding properties, the desired properties of the ECC composites, the durability needed, the desired sustainability of the system and the economic constraints of the application. (Lee et al 2010).

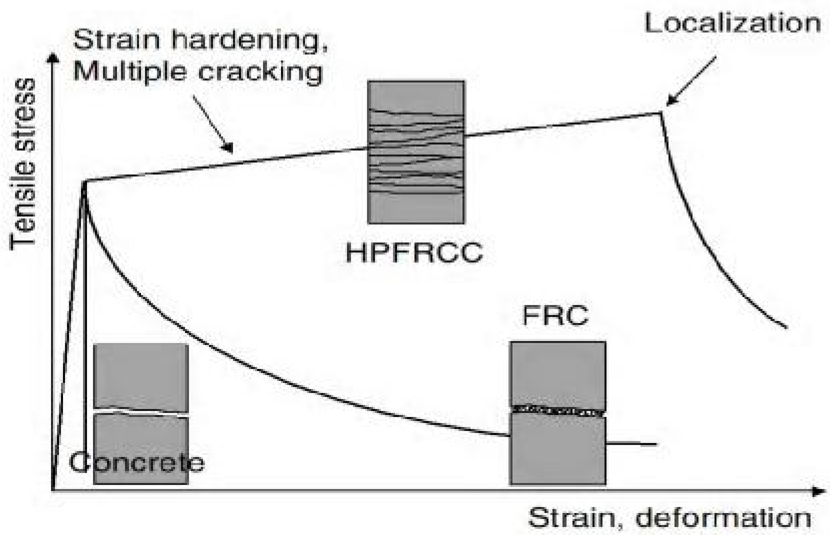


Fig. 1. Tensile stress-strain curves of concrete, FRC and HPFRCC (Fischer and Li 2000)

Table 1. Major physical properties of ECC (Li 2007)

| **Compressive Strength (MPa)** | **First Cracking Strength (MPa)** | **Ultimate Tensile Strength (MPa)** | **Ultimate Tensile Strain(%)** | **Young's Modulus (GPa)** | **Flexural Strength (MPa)** | **Density (gr/cc)** |
|---|---|---|---|---|---|---|
| 20-95 | 3-7 | 4-12 | 1-8 | 18-34 | 10-30 | 0.95-2.3 |

The plastic hinge rotation ($q_P$) of RC beams depends on a number of parameters including the definition of yielding and ultimate curvatures, section geometry, material properties, steel reinforcement ratios, transverse reinforcement, cracking and tension-stiffening, the stress-strain curve for the concrete in tension and compression, the stress-strain curve for the reinforcing steel, bond-slip characteristics between the concrete and the reinforcing steel, support conditions and the magnitude and type of loading, axial force, width of the loading plate, influence of shear, and the presence of column (Kheyroddin 1996). Some equations have been proposed to calculate the plastic hinge length ($l_P$) and the inelastic rotation capacity; however, there is no general agreement on the techniques to evaluate the inelastic characteristics of indeterminate concrete structures. The conditions at the ultimate load stage of a typical cantilever beam subjected to uniform load are shown in Fig. 2. For values of loads smaller than the yielding moment ($M_y$), the curvature is increasing gradually from the free end of a cantilever (point A) to the column face (point B). There is a large increase in the curvature at first yield of the tension steel. At the ultimate load stage, the value of the curvature at the support increases suddenly so that it causes large inelastic deformations (Kheyroddin and Naderpour 2007).

As it shown in Fig. 2(c), the actual distribution of curvature at the ultimate load stage can be idealized into elastic and plastic regions, thus the total rotation ($q_{total}$) over the beam length can be divided into elastic ($q_e$) and plastic ($q_P$) rotations. The elastic rotation which is defined until the first yielding of steel can be obtained using the curvature at yielding. The plastic hinge rotation ($q_P$) on each side of the critical section shown in Fig. 2, can be defined as:

$$q_P = \int_0^{l_y} \left[ f(x) - f_y \right] \cdot dx$$

Eq(1)

In which, $l_y$ is the beam length over which the bending moment is larger than the yielding moment ($M_y$) or the distance between the critical section and the location where tension steel bars start yielding and $f(x)$ is the curvature at a distance x from the critical section at the ultimate load stage. The shaded area in Fig. 1(c) shows the plastic rotation ($q_P$) that occurred in addition to the elastic rotation at the plastic hinge at the ultimate load stage. The plastic hinge rotation can be determined either by the calculation of shaded area or by an equivalent rectangle of height $(f_u - f_y)$ and width $l_P$. Equivalent plastic hinge length ($l_P$) can be defined as:

$$l_P = \frac{1}{f_u - f_y}\int_0^{l_y}\left[f(x) - f_y\right]\cdot dx$$

Eq(2)

Therefore, the value of plastic hinge rotation at the ultimate stage ($q_P$) can be calculated by the following equation:

$$q_P = (f_u - f_y)\cdot l_P = f_P \cdot l_P$$

Eq(3)

Where $f_u$ and $f_y$ are the curvatures at the ultimate load and yielding, respectively and $l_P$ is the equivalent length of the plastic hinge over which the plastic curvature ($f_P$), is assumed to be constant (Kheyroddin 1996).

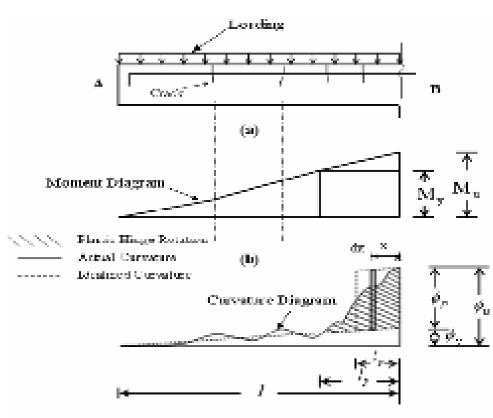


Fig. 2. Curvature distribution along a beam at ultimate stage (Kheyroddin 1996)

In this paper, an experimental work was carried out and then a nonlinear finite element program was used for performing a parametric study to examine the influence of compressive strength of HPFRCC, tension reinforcement ratio and the loading type on the ultimate deformation characteristics of reinforced HPFRCC beams and new equation is developed to consider the influence of the various parameters on the calculation of the ultimate curvature, yielding length, plastic hinge length and the plastic hinge rotation of these beams.

## b. Experimental program

An experimental investigation was undertaken to corroborate the analytical work and lend further insight into the nature of finite element items in beam analysis. The test specimens which were chosen for this analytical study were two large scale beams with two hinged supports which have been tested by authors. The beam clear span was 2100 mm, total length was 2300 mm with constant cross section of 300 mm deep by 200 mm wide. Two-point loading which was increased monotically, applied on this beam. Details of reinforcement layout and loading of the beam are shown in Fig. 3. Material properties are summarized in Table 2.

Test set up of RC and RHPFRCC beams is presented in Fig. 4. The amount of damage is more sever in RHPFRCC beam compared to RC beam as it shown in Fig. 5 and Fig. 6. Moreover, the mid-span deflection of RHPFRCC beam is more than RC beam. In RC beam, the ultimate load and mid-span deflection were 239.83 kN and 30.25 mm. While, in RHPFRCC beam, these values are 263.17 kN and 59.95 mm respectively.

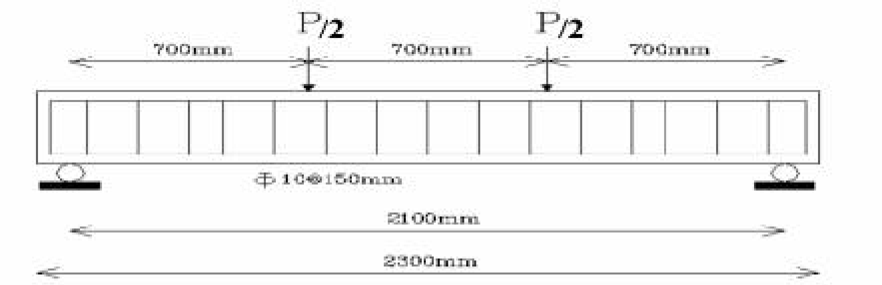


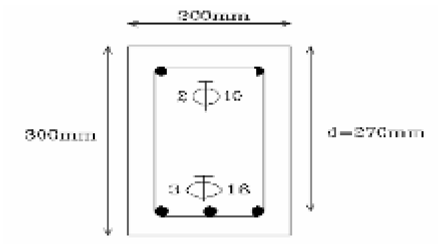


Fig. 3. Details of the experimental specimen

Table 2. Concrete, HPFRCC and steel properties used in the test beam

| Dimensions and material properties | (RC beam) | (HPFRCC beam) |
|---|---|---|
| $d$ $(mm)$ | 270 | 270 |
| $A_s$ $(mm^2)$ | 603 | 603 |
| $A'_s$ $(mm^2)$ | 157 | 157 |
| $f'_c$ $(MPa)$ | 35.7 | 24 |
| $e_{cu}$ * | 0.0075 | 0.0113 |
| $f_y$ $(MPa)$ | 400 | 400 |
| $E_s$ $(MPa)$ | 200,000 | 200,000 |
| $e_{su}$ | 0.02 | 0.02 |

* Assumed values

Fig. 4. Test Set-up

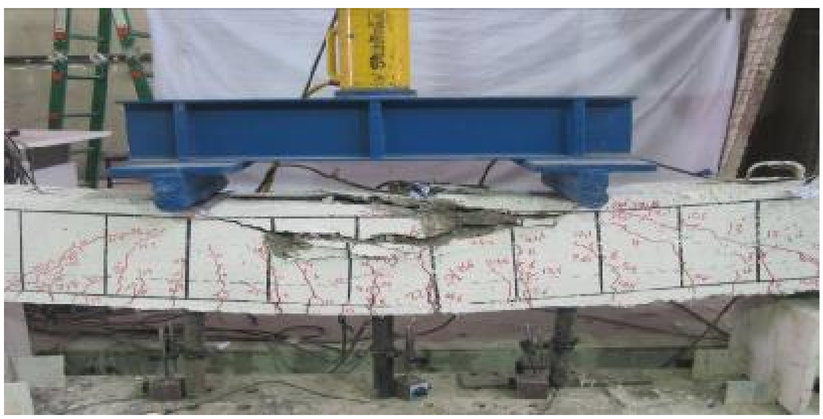

Fig. 5. RC beam at the end of test loading

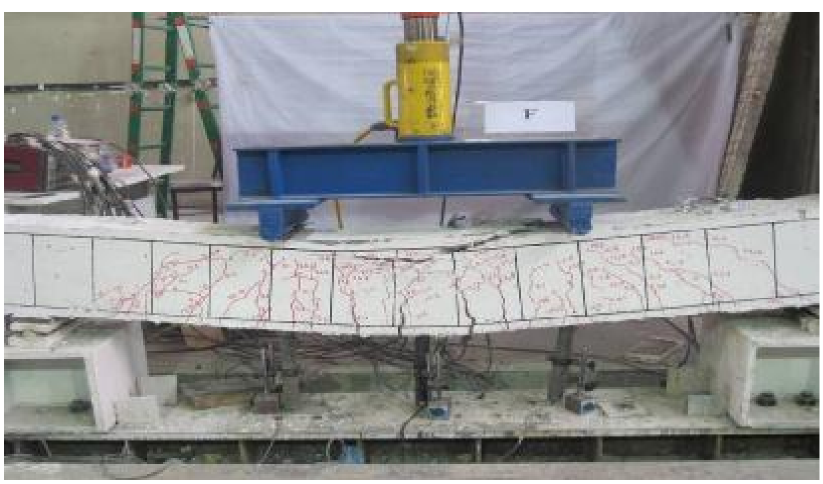


Fig. 6. RHPFRCC beam at the end of test loading

## c. Nonlinear finite element program and calibration

The beams were analyzed using the nonlinear finite element software called ABAQUS. This software is a powerful engineering simulation program, based on the finite element method that can perform nonlinear analyses. In a nonlinear analysis, ABAQUS automatically chooses appropriate load increments and convergence tolerances and continually adjusts them during the analysis to ensure that an accurate solution is obtained efficiently (ABAQUS 2008).

The reinforcing bars were modeled as an elastic strain hardening material by a 2 node nonlinear truss element shown in Fig. 7.

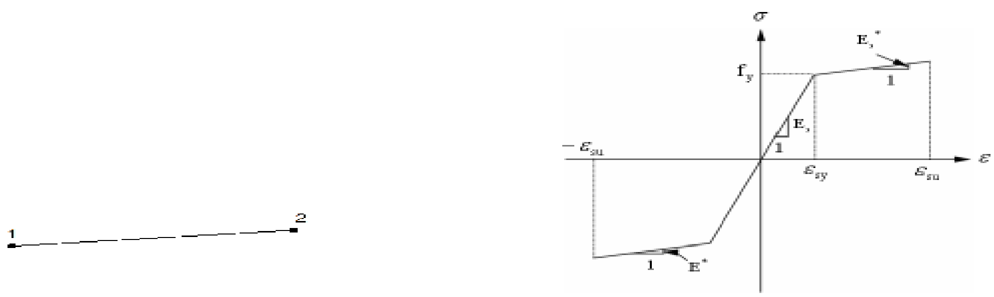


Fig. 7. Stress-strain curve and nonlinear element of reinforcing bars (ABAQUS 2008)

In this paper, concrete damage plasticity was selected for modeling of concrete and HPFRCC materials. The actual stress-strain curve of HPFRCC which was presented by various researchers and is close to regular concrete could be entered in damage plasticity model and calibrated with experimental work (Han et al 2003, Hung and El-Tawil 2010). The model is a continuum, plasticity-based, damage model for concrete. It was assumed that the main two failure mechanisms were tensile cracking and compressive crushing of the concrete material. The evolution of the yield (or failure) surface was controlled by two hardening variables ($\tilde{e}_t^{pl}$ and $\tilde{e}_c^{pl}$) linked to failure mechanisms under tension and compression loading, respectively. The model was assumed that the uni-axial tensile and compressive response of concrete was characterized by damaged plasticity, as shown in Fig. 8 (ABAQUS 2008). Where, $e_t$ and $e_c$ are tensile and compressive strain respectively. Some researchers have been developed other plasticity based models for HPFRCC material too (Kabele and Horii 1996, Sirijaroonchai 2009).

If $E_0$ is the initial (undamaged) elastic stiffness of the material, the stress-strain relations under uni-axial tension and compression loading are introduced by Eq. (4):

$$s_t = (1 - d_t) E_0 \left( e_t - \tilde{e}_t^{pl} \right)$$

$$s_c = (1 - d_c) E_0 \left( e_c - \tilde{e}_c^{pl} \right)$$

Eq. (4)

Where, $d_t$ and $d_c$ are two damage variables in tension and compression (0 = undamaged material and 1 = total loss of strength).

The concrete and HPFRCC were modeled as elastic strain softening and elastic strain hardening materials in tension as shown in Fig. 8 and Fig. 9 respectively. A 3-D nonlinear solid element with the ability to modeling the composite sections was applied for modeling these beams (Fig. 10). The compression behavior of these two materials is similar to each other (Fukuyama et al 2000). As it shown in Fig. 9, $s_{cc}$ and $s_{pc}$ are the first cracking stress and the maximum stress of HPFRCC with PVA fibers in the range of 0.75%-2% and are expressed by Eq. (5) (Suwannakarn 2009):

$$s_{cc} = s_{mu}\left(1 - V_f\right) + 0.5204 t V_f \, {}^{L}\!/_{d}$$

$$s_{pc} = (-0.7074 V_f + 2.0933) t V_f \, {}^{L}\!/_{d}$$

Eq. (5)

Where, $s_{mu}$ = Tensile strain of matrix, $V_f$ = Volume fraction of fiber, $t$ = Average bond strength at the fiber matrix interface, $L$ = Fiber length and $d$ = Fiber diameter.

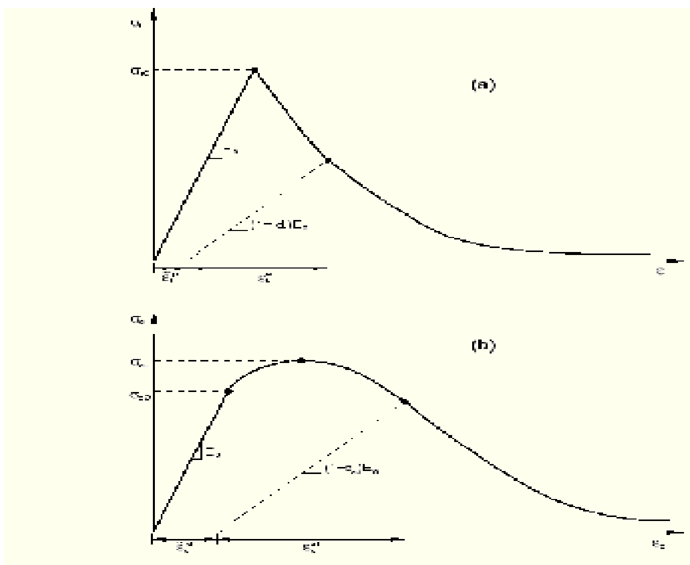


Fig. 8. Response of concrete in (a) tension and (b) compression (ABAQUS 2008)

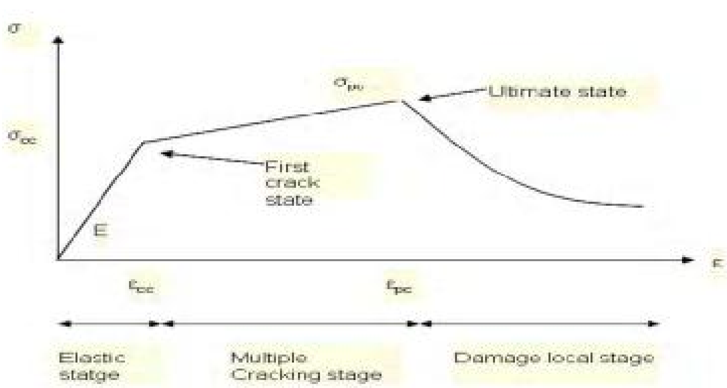


Fig. 9. Tensile behavior of HPFRCC (Fukuyama et al 2000)

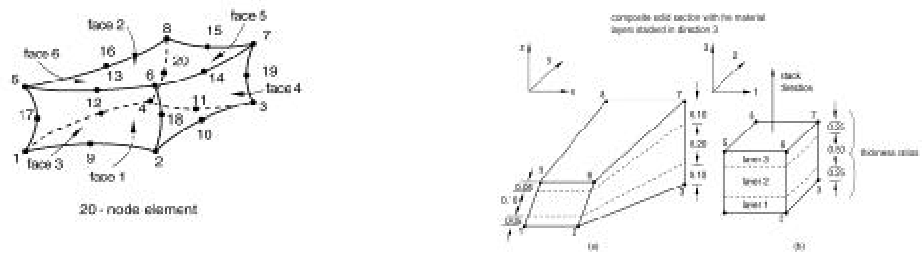


Fig. 10. Nonlinear element for modeling of concrete and HPFRCC (ABAQUS 2008)

In this research, two beams (RC and RHPFRCC beams) are analyzed using ABAQUS program. To investigate the influence of mesh size on the nonlinear analysis results, three types of mesh configurations were used for analyzing these beams. These mesh configurations including coarse, medium and fine mesh sizes. Load-mid span deflection curves for these two RC and RHPFRCC beams are shown in Fig. 11 and Fig. 12.

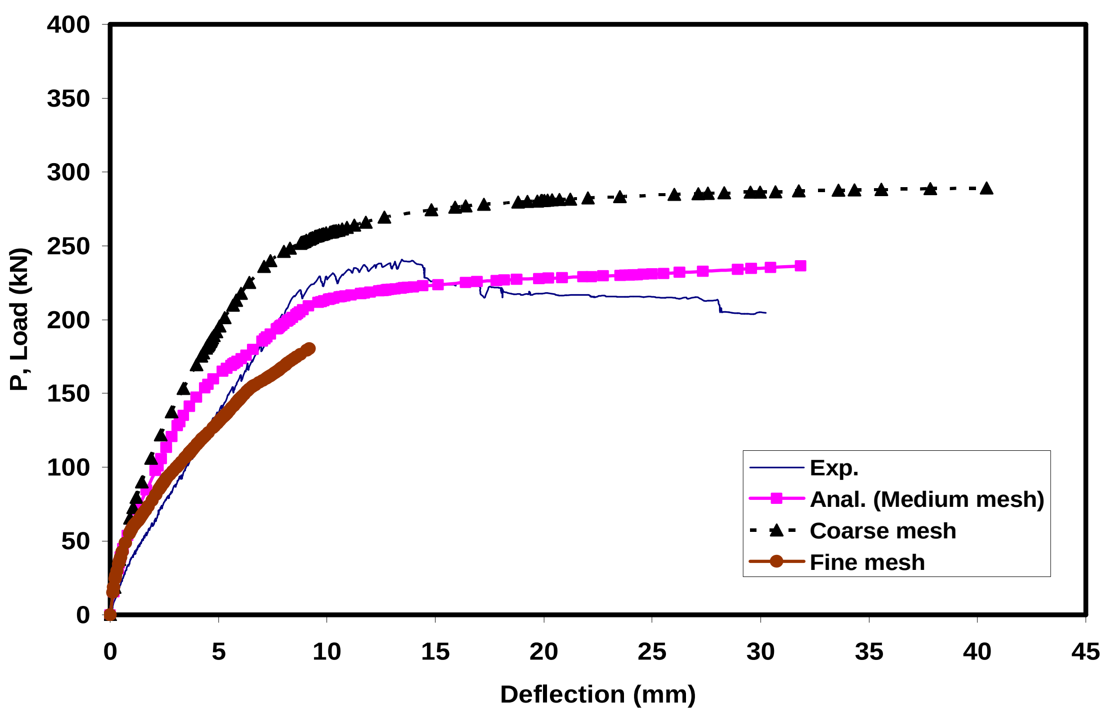


Fig. 11. Load-mid span deflection curves for different mesh sizes in RC beam

In RC beams, the medium mesh size (50mm x 50mm), gave an ultimate load value of 236.46 kN, which was close to the experimental value 239.83 kN. While the coarse mesh size (100mm x 100mm), results in an ultimate load value 289.17 kN and the fine mesh size (25mm x 25mm), concludes to an ultimate load 180.44 kN. Both of these values are far from the experimental value. In HPFRCC beams, the medium mesh size (50mm x 50mm) gave an ultimate load value of 259.5 kN, which was close to the experimental value 263.17 kN. While the coarse mesh size results in an ultimate load value 334.26 kN and the fine mesh size concludes to an ultimate load 220 kN. Both of these values are far from the experimental value. These analytical results are summarized in Table 3 and Table 4.

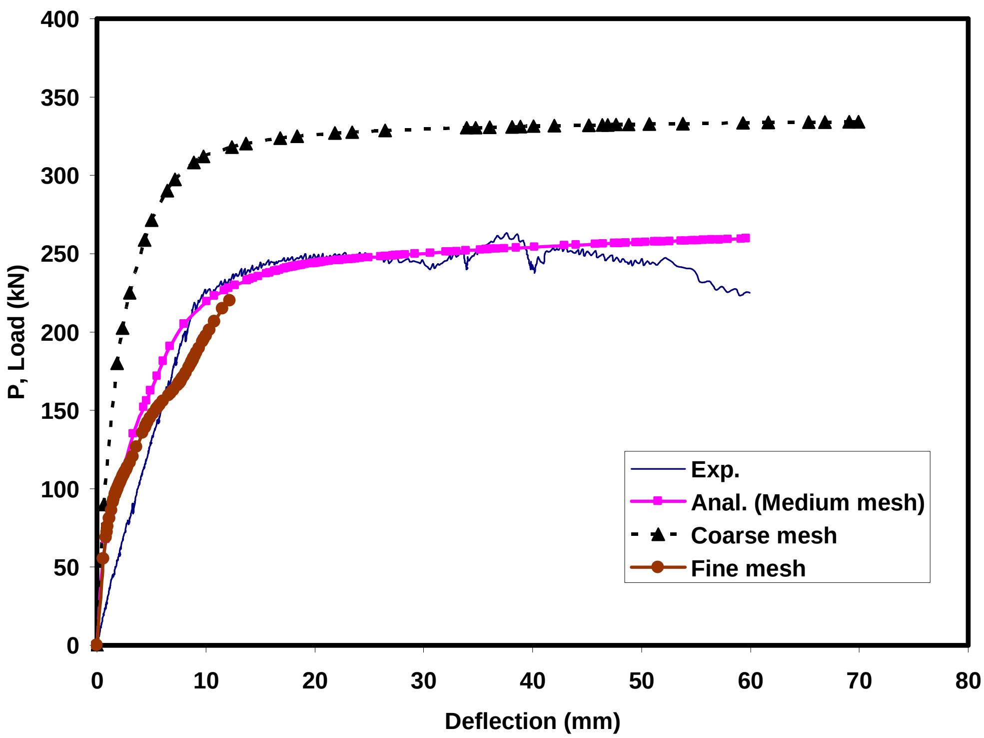


Fig. 12. Load-mid span deflection curves for different mesh sizes in HPFRCC beam

Table 3. Analytical and experimental results for RC beams with different mesh sizes

| Size of elements (mm x mm) | $P_u$ (kN) | $\Delta_u$ (mm) | $\frac{P_u(Analytical)}{P_u(Experimental)}$ |
|---|---|---|---|
| Experimental | 239.83 | 30.25 | - |
| 25 x 25 | 180.44 | 9.18 | 0.75 |
| 50 x 50 | 236.46 | 31.84 | 0.98 |
| 100 x 100 | 289.17 | 40.43 | 1.21 |

Table 4. Analytical and experimental results for HPFRCC beams with different mesh sizes

| Size of elements (mm x mm) | $P_u$ (kN) | $\Delta_u$ (mm) | $\frac{P_u(Analytical)}{P_u(Experimental)}$ |
|---|---|---|---|
| Experimental | 263.17 | 59.95 | - |
| 25 x 25 | 220 | 12.18 | 0.84 |
| 50 x 50 | 259.5 | 59.61 | 0.98 |
| 100 x 100 | 334.26 | 69.93 | 1.27 |

As can be seen in Fig. 11 and Fig. 12, when a coarse mesh size is applied, the beam exhibits a stiffer behavior compared with the experimental response. With increasing the number of elements, the beam trends to be more flexible and less ductile. Infact, the mid span deflection at ultimate load decreases with reducing in element size. Hence, medium mesh size is selected for analytical purposes. Cracking is idealized using the smeared cracking model, and assumed to occur when the principal tensile stress at a point (usually a Gauss integration point) exceeds the concrete tensile strength. The stiffness across the crack is assumed to be zero and the principal directions are not allowed to rotate. For evaluation of an "appropriate" value of the ultimate tensile strain of the concrete, $e_{tu}$, and elimination of mesh size dependency phenomenon, Shayanfar et al. proposed the following simple formula:

$$e_{tu} = 0.004 \cdot e^{-0.058\,h} \qquad \text{Eq. (6)}$$

Where, h is the width of the element in mm. In concrete materials, finer mesh size does not always conclude to more exact response and there is a limit value for this case. Decreasing in element size of concrete materials is concluded to more flexible beam and subsequently decreasing in ultimate force of the beam (Shayanfar et al 1996).

## d. Analytical models

The experimental HPFRCC beam, 200 x 300 mm, with a tension reinforcement ratio of 0.0112 and compressive strength of 24 MPa subjected to a two-point load, is used for the parametric study in this paper. In addition, the same beams were analyzed with four other assumed tension reinforcement ratios (0.022, 0.0147, 0.0074, and 0.006), another assumed compressive strength of 35.7 MPa (same to RC beam) under the three load types (two-point, concentrated and uniform). Model names are summarized in Table 5.

Table 5. Name of analytical models

| Model names | Description | $f_c'$ $(MPa)$ | Tension reinforcement ratio $(r)$ | Load type |
|---|---|---|---|---|
| RC1 | Reinforced concrete | 35.7 | 0.0112 | Two-point |
| RC2 | Reinforced concrete | 24 | 0.0112 | Two-point |
| RH1 | Reinforced HPFRCC | 24 | 0.0112 | Two-point |
| RH2 | Reinforced HPFRCC | 35.7 | 0.0112 | Two-point |
| RH3 | Reinforced HPFRCC | 24 | 0.0112 | Concentrated |
| RH4 | Reinforced HPFRCC | 24 | 0.0112 | Uniform |
| RH5 | Reinforced HPFRCC | 24 | 0.006 | Two-point |
| RH6 | Reinforced HPFRCC | 24 | 0.0074 | Two-point |
| RH7 | Reinforced HPFRCC | 24 | 0.0147 | Two-point |
| RH8 | Reinforced HPFRCC | 24 | 0.022 | Two-point |
| RH9 | Reinforced HPFRCC | 24 | 0.006 | Concentrated |
| RH10 | Reinforced HPFRCC | 24 | 0.0074 | Concentrated |
| RH11 | Reinforced HPFRCC | 24 | 0.0147 | Concentrated |
| RH12 | Reinforced HPFRCC | 24 | 0.022 | Concentrated |
| RH13 | Reinforced HPFRCC | 24 | 0.006 | Uniform |
| RH14 | Reinforced HPFRCC | 24 | 0.0074 | Uniform |
| RH15 | Reinforced HPFRCC | 24 | 0.0147 | Uniform |
| RH16 | Reinforced HPFRCC | 24 | 0.0022 | Uniform |

# e. Results and Discussion

## e.1. Two-point loading

### e.1.1. Compressive strength effect

Load deflection curves of RH1 and RH2 are illustrated in Fig. 13. Load deflection curves of RC1 and RC2 are illustrated in Fig. 14. The analytical results including the yielding and ultimate loads, deflections and curvatures and ductility ratios for these beams are also presented in Table 5. The mode of failure is flexural for all beams, i.e., steel reinforcements yield prior compressive HPFRCC and concrete crushing. As shown in these figures and tables, ultimate load, deflection, curvature and ductility ratio of RH2 beam are about 0.7 %, 1.58 %, 1.8 % and 0.2 % higher than its corresponding values in RH1 beam. In RC1 beam, the ultimate load, deflection, curvature and ductility ratio are about 1 %, 3.6 %, 8.3 % and % 8.3 % more than RC2 respectively. Load and deflection capacity, curvature and ductility ratio of reinforced concrete and HPFRCC beams increase with increasing the compressive strength of concrete and HPFRCC. It seems that these parameters in reinforced HPFRCC beams are higher than corresponding values in reinforced concrete beams.

For calculating the of $q_p$ and $l_p$ values, the curvature along the beam is obtained from the concrete and HPFRCC strain values in compression zone and from the steel strain in tension zone at the ultimate limit state. Then the $q_p$ is calculated by integration along the yielding length. Curvature distribution in RH1 and RH2 beams and also in RC1 and RC2 beams are presented in Fig. 15 and Fig. 16. Plastic hinge characteristics including the yielding length ($l_y$), plastic hinge length ($l_p$) and plastic hinge rotation ($q_p$) of these beams are also presented in Table 6. As it shown in Fig. 15, the maximum value of curvature is occurred in the distance of about 400 mm and 350 mm from mid-span of the RH1 and RH2 beams which are very close to the point of two concentrated loads (the distance between two concentrated loads in these beams are 700 mm). In the case of RC1 and RC2 beams, the maximum value of curvature is occurred in distance of about 250 mm and 300 mm from mid-span of the RC1 and RC2 beams. As it shown in Table 6, in the case of reinforced concrete and reinforced HPFRCC beams, increasing in the compressive strength concludes to an increase in $l_p$ and $q_p$ values. Plastic hinge length and plastic hinge rotation of RH2 beam are about 0.6 % and 1.8 % higher than its corresponding values in RH1 beam. In RC1 beam, plastic hinge length and plastic hinge rotation are about 3 % and 13 % more than RC2 respectively. It is obvious that these parameters in reinforced HPFRCC beams are higher than corresponding values in reinforced concrete beams. As it shown in Table 5, plastic hinge length and rotation of RHPFRCC beams are about 1.065 and 1.77 times more than RC beams. But the yield length in both beams is the same approximately.

This may be due to existence of reinforcing fibers, HPFRCC material maintains its unity under sever loading (bridging mechanism and pull out of fibers) and subsequently steel reinforcements suffer more strains and reach more close to the value of their plastic strain. Moreover, the ultimate compressive strain of HPFRCC is more than normal concrete. This phenomenon concludes to increase in ultimate curvature, plastic hinge length and plastic hinge rotation of RHPFRCC beams capacity of HPFRCC beams compared to RC beams.

Table 5. Analytical results for RH1, RH2, RC1 and RC2 beams

| Model name | $P_y$ (kN) | $\Delta_y$ (mm) | $P_u$ (kN) | $\Delta_u$ (mm) | $f_y \times 10^{-6}$ (rad/mm) | $f_u \times 10^{-6}$ (rad/mm) | $m_\Delta = \frac{\Delta_u}{\Delta_y}$ | $m_f = \frac{f_u}{f_y}$ |
|---|---|---|---|---|---|---|---|---|
| RH1 | 236.43 | 10.36 | 259.5 | 59.61 | 26.2 | 87.4 | 5.75 | 3.34 |
| RH2 | 238.6 | 10.4 | 261.49 | 60.55 | 26.6 | 89 | 5.82 | 3.35 |
| RC1 | 217.26 | 10.17 | 236.46 | 31.84 | 18.8 | 59 | 3.13 | 3.14 |
| RC2 | 221.25 | 9.98 | 2234.12 | 30.73 | 18.8 | 54.5 | 3.08 | 2.9 |

Table 6. Plastic hinge characteristics of RH1, RH2, RC1 and RC2 beams

| Model name | $l_y$ (mm) | $l_p$ (mm) | $q_p$ (rad) | $\frac{l_p}{(l_p)_{RC2}}$ | $\frac{q_p}{(q_p)_{RC2}}$ |
|---|---|---|---|---|---|
| RH1 | 550 | 290 | 0.0223 | 1.062 | 1.756 |
| RH2 | 550 | 292 | 0.0227 | 1.069 | 1.787 |
| RC1 | 550 | 281 | 0.0143 | 1.029 | 1.126 |
| RC2 | 550 | 273 | 0.0127 | 1 | 1 |

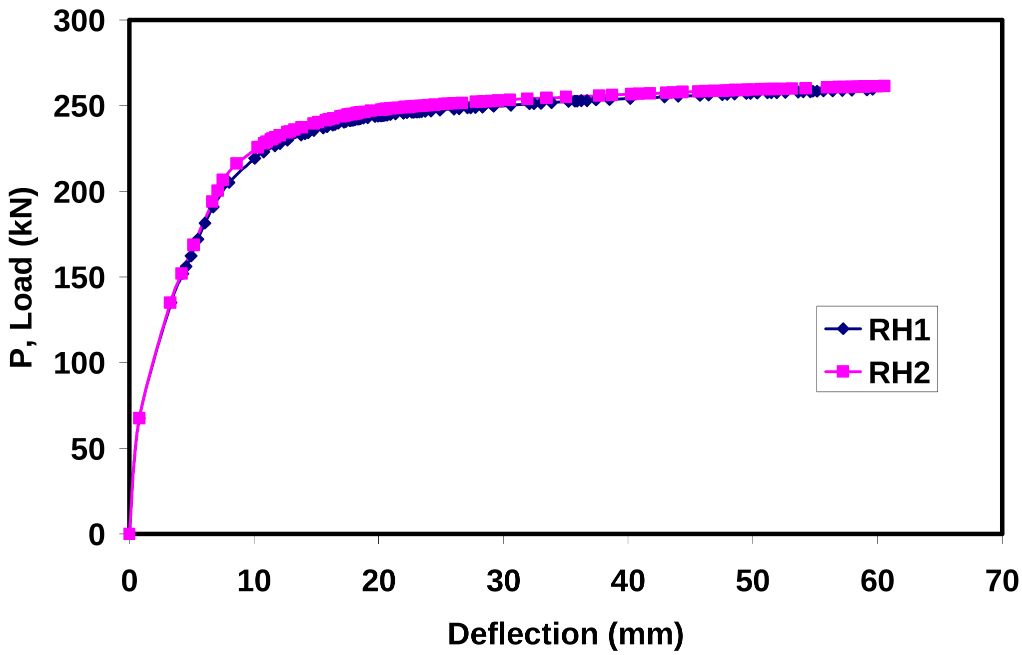


Fig. 13. Load-deflection curves of RH1 and RH2 beams

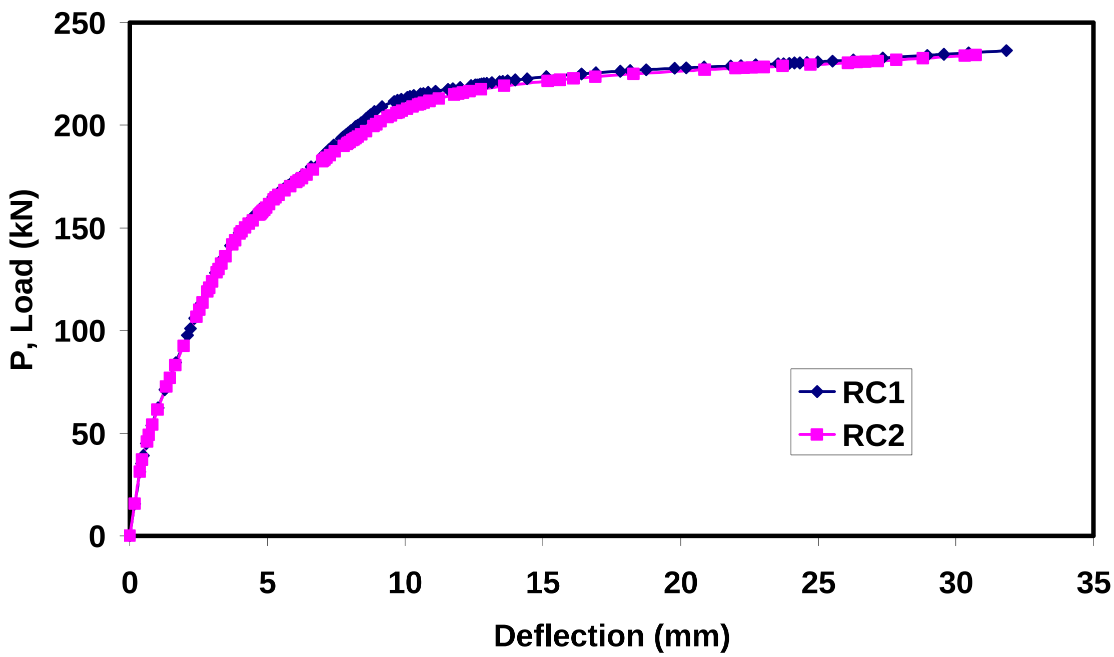


Fig. 14. Load-deflection curves of RC1 and RC2 beams

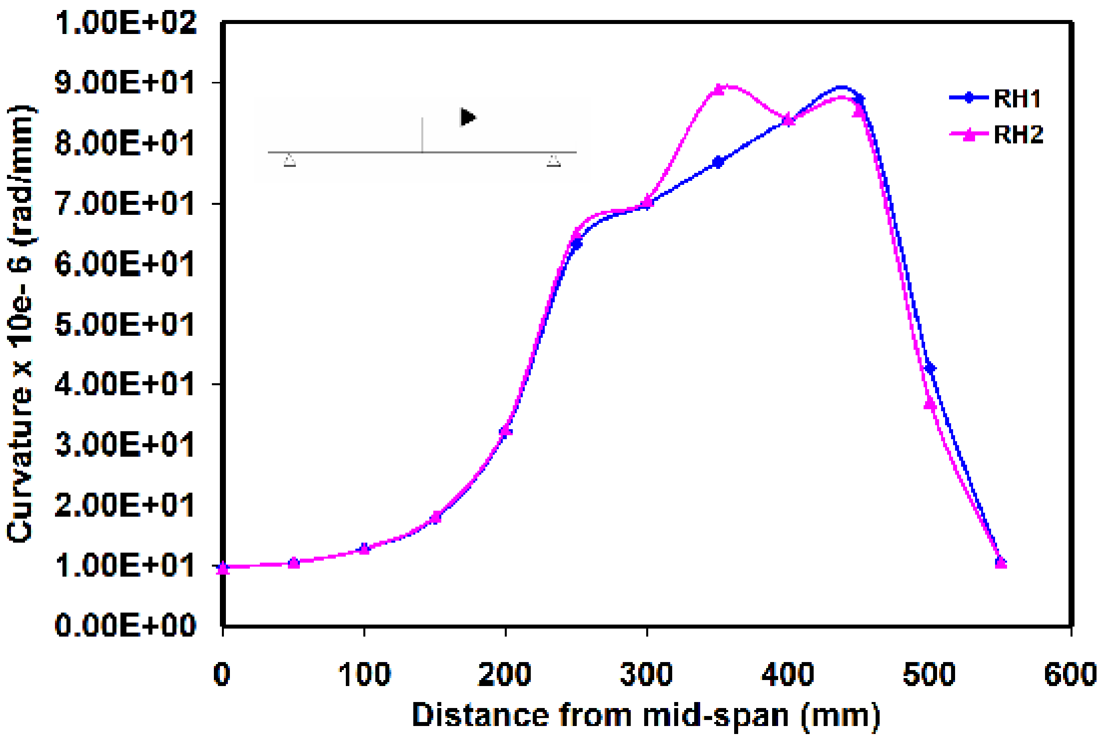


Fig. 15. Distribution of curvature in RH1 and RH2 beams

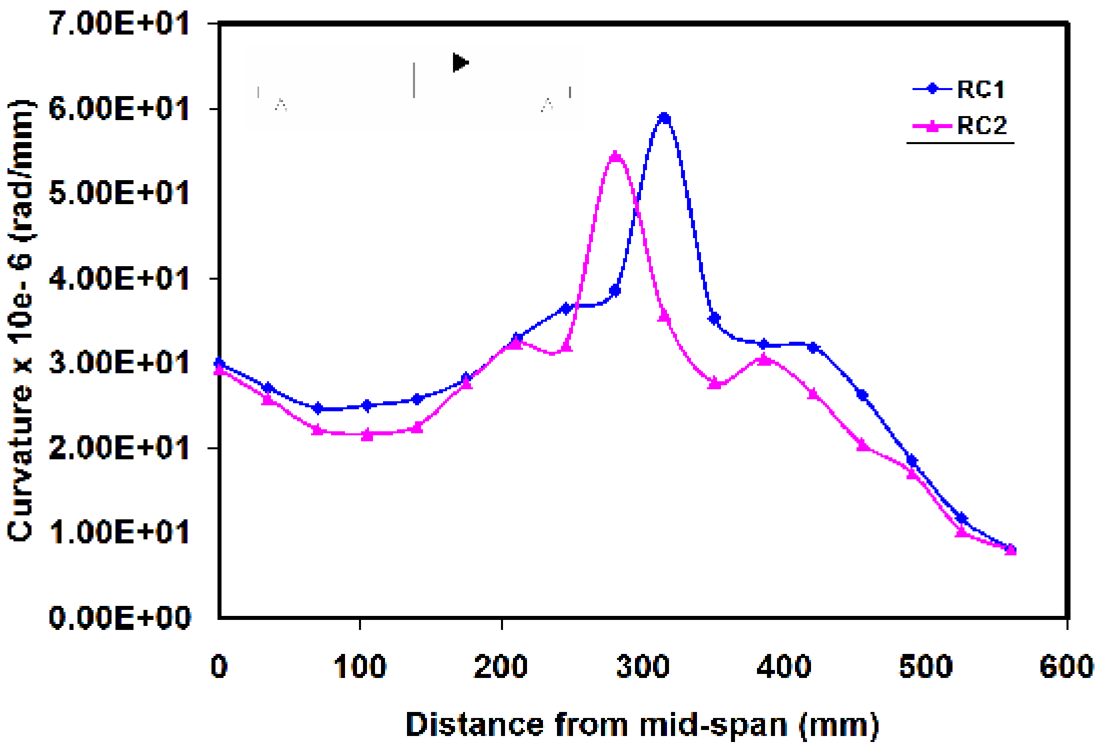


Fig. 16. Distribution of curvature in RC1 and RC2 beams

**e.1.2. Influence of tension reinforcement ratio**

Load deflection curves of RH1, RH5, RH6, RH7 and RH8 beams are illustrated in Fig. 17. The analytical results including the yielding and ultimate loads, deflections and curvatures and ductility ratios for these beams are also presented in Table 7. The mode of failure is flexural for all of these beams. As it shown in Fig. 17 and Table 7, increasing in the value of tension reinforcement ratio in these beams conclude to higher ultimate load values. In the other hand, increasing in the value of tension reinforcement ratio of these beams conclude to less ultimate deflection, curvature and ductility ratio.

Distribution of curvature in RH1, RH5, RH6, RH7 and RH8 are presented in Fig. 18. As it shown in this figure, the maximum value of curvature is occurred in the distance of about 400 mm from mid-span of the RH1 and RH2 beams which is very close to the point of two concentrated loads (the distance between two concentrated loads in these beams are 700 mm). Plastic hinge characteristics of these beams are also presented in Table 6. It seems that increasing in the value of tension reinforcement ratio of these beams conclude to less plastic hinge length and plastic hinge rotation. The plastic hinge length of RH5, RH6, RH7 and RH8 are about 1.028, 1.01, 0.996 and 0.883 times to the value obtained for RH1 beam. The plastic hinge rotation of RH5, RH6, RH7 and RH8 are about 1.386, 1.224, 0.919 and 0.619 times to the value obtained for RH1 beam.

As it shown in Table 8, plastic hinge length and rotation of RHPFRCC beams are about 1.05 and 1.8 times more than RC beams. But the yield length in both beams is the same approximately.

Table 7. Analytical results for RH1, RH5, RH6, RH7 and RH8 beams

| Model name | $P_y$ (kN) | $\Delta_y$ (mm) | $P_u$ (kN) | $\Delta_u$ (mm) | $f_y \times 10^{-6}$ (rad/mm) | $f_u \times 10^{-6}$ (rad/mm) | $m_\Delta = \frac{\Delta_u}{\Delta_y}$ | $m_f = \frac{f_u}{f_y}$ |
|---|---|---|---|---|---|---|---|---|
| RH1 | 236.43 | 10.36 | 259.5 | 59.61 | 26.2 | 87.4 | 5.75 | 3.34 |
| RH5 | 176.72 | 7.71 | 228.62 | 69.21 | 19 | 114 | 8.98 | 6 |
| RH6 | 195.29 | 8.84 | 239.61 | 63.21 | 21.2 | 104 | 7.15 | 4.91 |
| RH7 | 277.26 | 11.15 | 310.66 | 39.72 | 28.8 | 79.8 | 3.56 | 2.77 |
| RH8 | 333.64 | 16.14 | 349.48 | 33.51 | 32.8 | 63.5 | 2.03 | 1.94 |

Table 8. Plastic hinge characteristics of RH1, RH5, RH6, RH7 and RH8 beams

| Model name | $l_y$ (mm) | $l_p$ (mm) | $q_p$ (rad) | $\frac{l_p}{(l_p)_{RC2}}$ | $\frac{q_p}{(q_p)_{RC2}}$ |
|---|---|---|---|---|---|
| RH1 | 550 | 290 | 0.0223 | 1.062 | 1.756 |
| RH5 | 550 | 298 | 0.0309 | 1.091 | 2.433 |
| RH6 | 550 | 293 | 0.0273 | 1.073 | 2.149 |
| RH7 | 550 | 289 | 0.0205 | 1.058 | 1.614 |
| RH8 | 450 | 256 | 0.0138 | 0.938 | 1.086 |

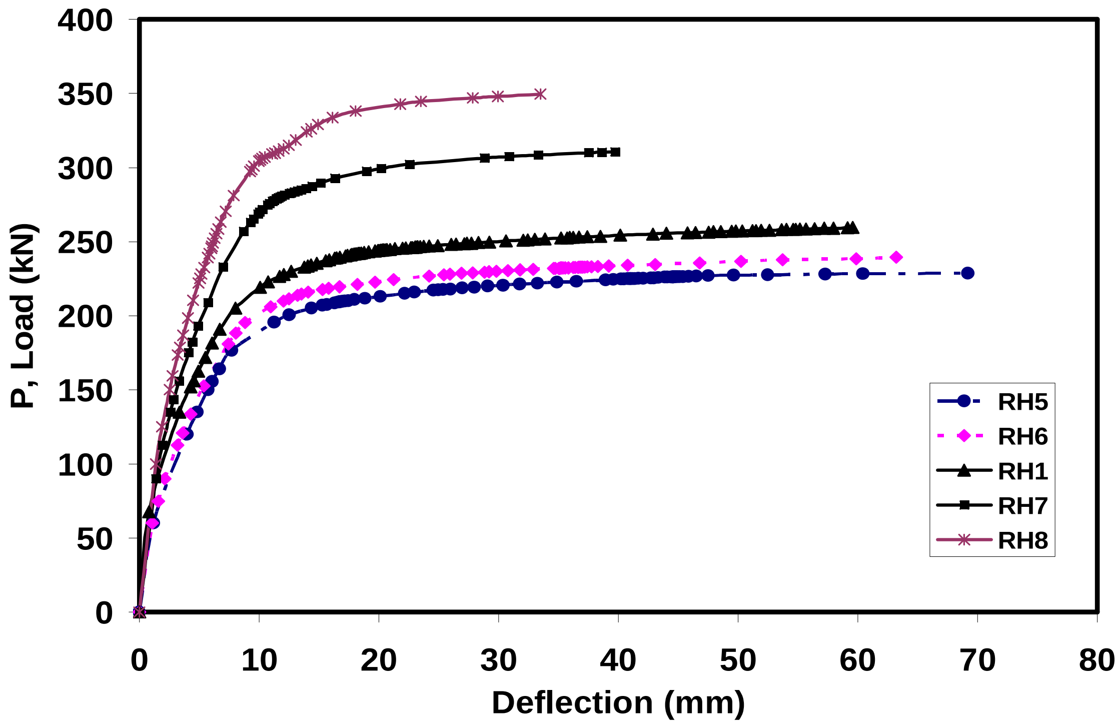


Fig. 17. Load-deflection curves of RH1, RH5, RH6, RH7 and RH8 beams

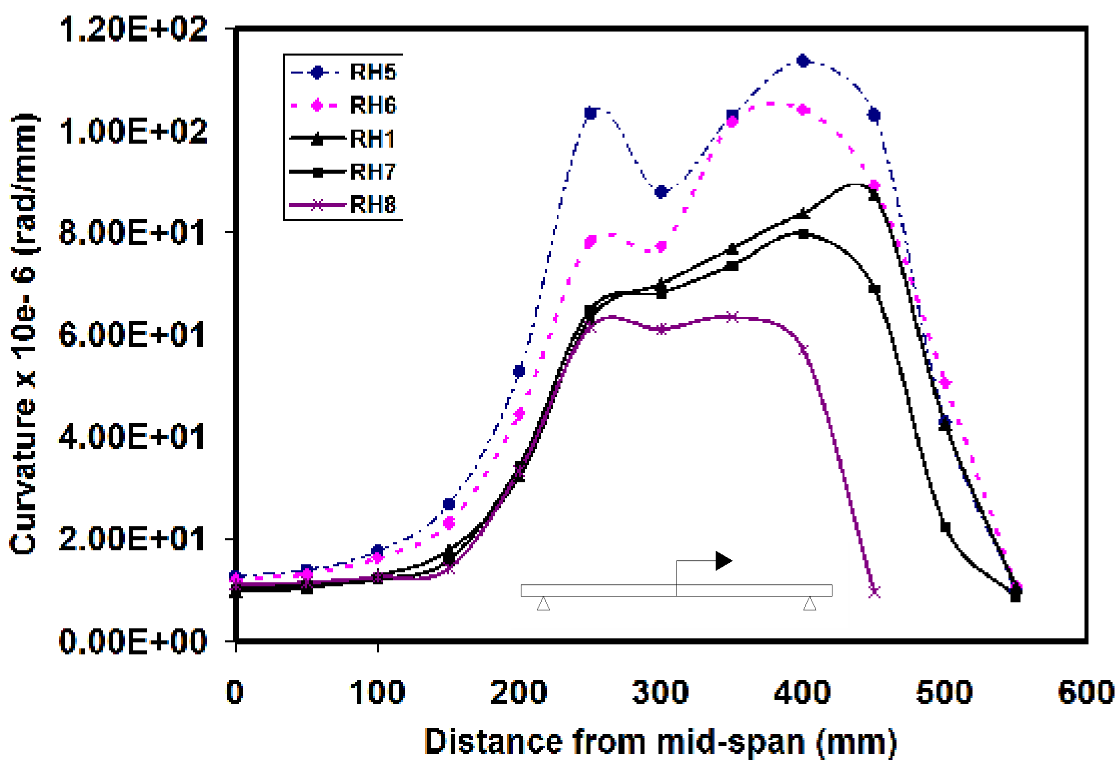


Fig. 18. Distribution of curvature in RH1, RH5, RH6, RH7 and RH8 beams

## e.2. Concentrated loading

### e.2.1. Influence of tension reinforcement ratio

Load deflection curves of RH3, RH9, RH10, RH11 and RH12 beams are illustrated in Fig. 19. The analytical results for these beams are presented in Table 9. Distribution of curvature in RH3, RH9, RH10, RH11 and RH12 are presented in Fig. 20. Plastic hinge characteristics of these beams are also presented in Table 10.

As it shown in these figures and tables, increasing in the value of tension reinforcement ratio in these beams conclude to higher ultimate load values. In the other hand, increasing in the value of tension reinforcement ratio of these beams conclude to less ultimate deflection, curvature and ductility ratio. The maximum value of curvature is occurred in the mid span of these beams, i.e., at the point of concentrated load. It seems that increasing in the value of tension reinforcement ratio of these beams conclude to less plastic hinge length and plastic hinge rotation.

In the case of reinforced HPFRCC beams under concentrated load, ultimate deflection, curvature and ductility ratio are higher compared to corresponding beams subjected to two-point loading. But, plastic hinge length and rotation is less than two-point loading beams. The plastic hinge length of RH3, RH9, RH10, RH11 and RH12 are about 0.683, 0.741, 0.724, 0.638 and 0.586 times to the value obtained for RH1 beam. The plastic hinge rotation of RH3, RH9, RH10, RH11 and RH12 are about 0.991, 1.13, 1.103, 0.87 and 0.605 times to the value obtained for RH1 beam.

As it shown in Table 8, plastic hinge length and rotation of RHPFRCC beams are about 0.72 and 1.65 times compared to RC beams under two-point loading.

Table 9. Analytical results for RH3, RH9, RH10, RH11 and RH12 beams

| Model name | $P_y$ (kN) | $\Delta_y$ (mm) | $P_u$ (kN) | $\Delta_u$ (mm) | $f_y \times 10^{-6}$ (rad/mm) | $f_u \times 10^{-6}$ (rad/mm) | $m_\Delta = \frac{\Delta_u}{\Delta_y}$ | $m_f = \frac{f_u}{f_y}$ |
|---|---|---|---|---|---|---|---|---|
| RH3 | 152.03 | 6.01 | 219.16 | 62.71 | 25.3 | 119 | 10.43 | 4.7 |
| RH9 | 110 | 5.21 | 180.31 | 76.8 | 19.3 | 125 | 14.74 | 6.48 |
| RH10 | 124.66 | 5.82 | 185 | 70.23 | 21.4 | 125 | 12.07 | 5.84 |
| RH11 | 190.98 | 7.36 | 237.31 | 48.84 | 29.4 | 114 | 6.64 | 3.88 |
| RH12 | 231.94 | 8.98 | 262.78 | 44.38 | 30.5 | 89.2 | 4.94 | 2.92 |

Table 10. Plastic hinge characteristics of RH3, RH9, RH10, RH11 and RH12 beams

| Model name | $l_y$ (mm) | $l_p$ (mm) | $q_p$ (rad) | $\frac{l_p}{(l_p)_{RC2}}$ | $\frac{q_p}{(q_p)_{RC2}}$ |
|---|---|---|---|---|---|
| RH3 | 350 | 198 | 0.0221 | 0.725 | 1.74 |
| RH9 | 350 | 215 | 0.0252 | 0.788 | 1.984 |
| RH10 | 350 | 210 | 0.0246 | 0.769 | 1.937 |
| RH11 | 300 | 185 | 0.0194 | 0.678 | 1.528 |
| RH12 | 250 | 170 | 0.0135 | 0.623 | 1.063 |

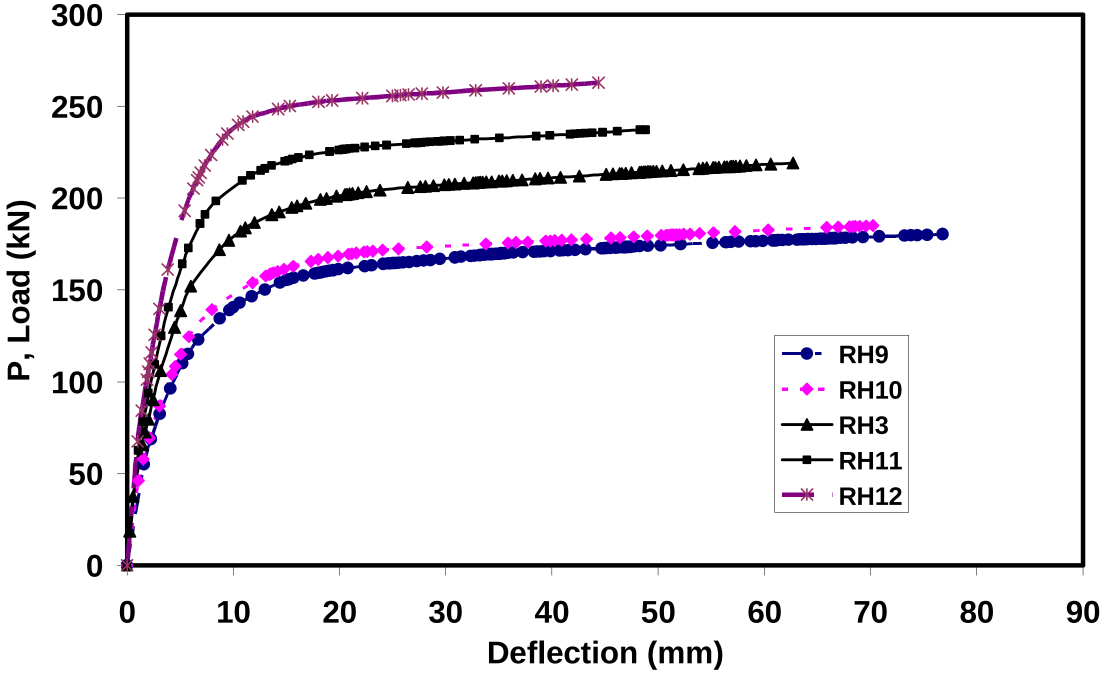


Fig. 19. Load deflection curves of RH3, RH9, RH10, RH11 and RH12 beams

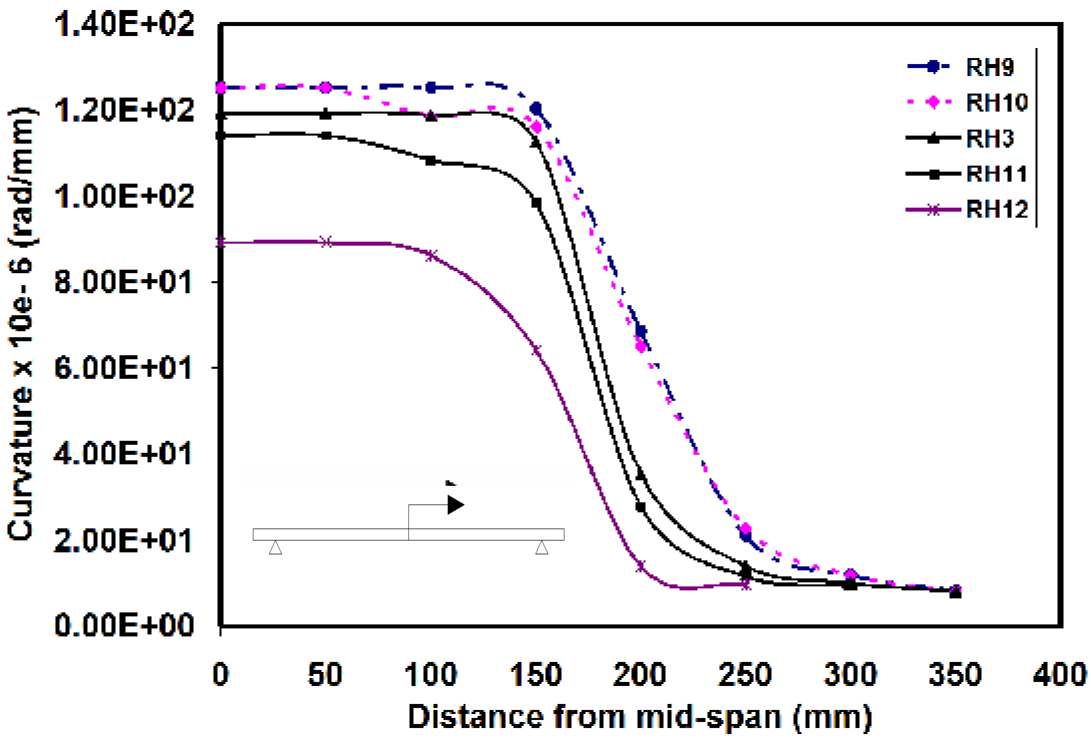


Fig. 20. Distribution of curvature in RH3, RH9, RH10, RH11 and RH12 beams

### e.3. Uniform loading

#### e.3.1. Influence of tension reinforcement ratio

Distribution of curvature in RH4, RH13, RH14, RH15 and RH16 are presented in Fig. 21. The analytical results for these beams are presented in Table 11. Plastic hinge characteristics of these beams are also presented in Table 12.

As it shown in these figures and tables, increasing in the value of tension reinforcement ratio in these beams conclude to higher ultimate load values. In the other hand, increasing in the value of tension reinforcement ratio of these beams conclude to less ultimate deflection, curvature and ductility ratio. The maximum value of curvature is occurred in the mid span of these beams, i.e., at the point of concentrated load. It seems that increasing in the value of tension reinforcement ratio of these beams conclude to less plastic hinge length and plastic hinge rotation.

In the case of reinforced HPFRCC beams under uniform load, plastic hinge length and rotation is lees than 2-point loading beams but more than concentrated loading beams. The plastic hinge length of RH3, RH9, RH10, RH11 and RH12 are about 0.845, 0.845, 0.817, 0.766 and 0.759 times to the value obtained for RH1 beam. The plastic hinge rotation of RH3, RH9, RH10, RH11 and RH12 are about 1.013, 1.287, 1.211, 0.879 and 0.61 times to the value obtained for RH1 beam.

As it shown in Table 8, plastic hinge length and rotation of RHPFRCC beams are about 0.86 and 1.76 times compared to RC beams under 2-point loading.

Distribution of curvature in RH1, RH3 and RH4 are presented in Fig. 22. As could be seen in this figure, the yielding length of 2-point loaded HPFRCC beam is longer than other beams. The ultimate curvature of concentrate loaded beam is greater than others.

The area under the curve of 2-point loaded HPFRCC beam is more than other beams and concluded to more $q_p$ and $l_p$ values.

Table 11. Analytical results for RH4, RH13, RH14, RH15 and RH16 beams

| Model name | $P_y$ (kN) | $\Delta_y$ (mm) | $P_u$ (kN) | $\Delta_u$ (mm) | $f_y \times 10^{-6}$ (rad/mm) | $f_u \times 10^{-6}$ (rad/mm) | $m_\Delta = \frac{\Delta_u}{\Delta_y}$ | $m_f = \frac{f_u}{f_y}$ |
|---|---|---|---|---|---|---|---|---|
| RH4 | 341.76 | 13.76 | 405.79 | 60.82 | 28.6 | 102 | 4.42 | 3.57 |
| RH13 | 258.8 | 8.34 | 343.91 | 70.01 | 19.3 | 125 | 8.39 | 6.48 |
| RH14 | 277.24 | 10.33 | 357.85 | 65.22 | 21.6 | 124 | 6.31 | 5.74 |
| RH15 | 423.65 | 19.8 | 445.26 | 41.14 | 29.5 | 96.4 | 2.08 | 3.27 |
| RH16 | 509.9 | 23.1 | 524.97 | 34.59 | 32.9 | 71.2 | 1.5 | 2.16 |

Table 12. Plastic hinge characteristics of RH4, RH13, RH14, RH15 and RH16 beams

| Model name | $l_y$ (mm) | $l_p$ (mm) | $q_p$ (rad) | $\frac{l_p}{(l_p)_{RC2}}$ | $\frac{q_p}{(q_p)_{RC2}}$ |
|---|---|---|---|---|---|
| RH4 | 500 | 245 | 0.0226 | 0.897 | 1.78 |
| RH13 | 550 | 245 | 0.0287 | 0.897 | 2.26 |
| RH14 | 500 | 237 | 0.027 | 0.868 | 2.126 |
| RH15 | 350 | 222 | 0.0196 | 0.813 | 1.54 |
| RH16 | 300 | 220 | 0.0136 | 0.806 | 1.071 |

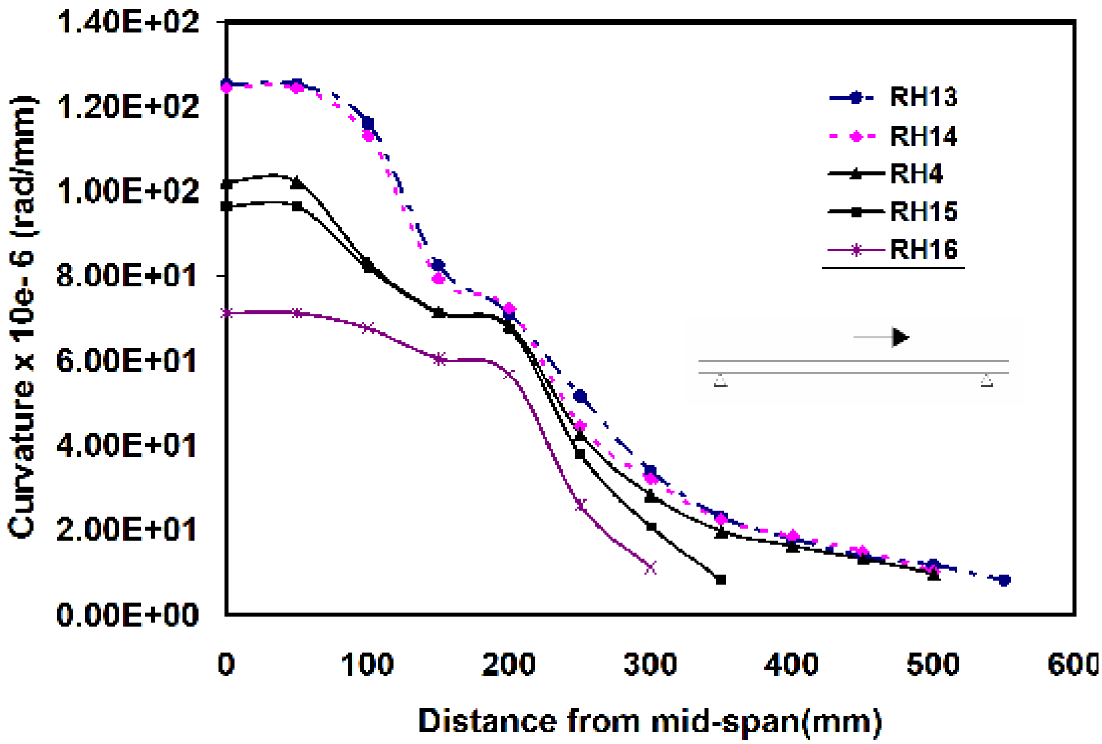


Fig. 21. Distribution of curvature in RH4, RH13, RH14, RH15 and RH16 beams

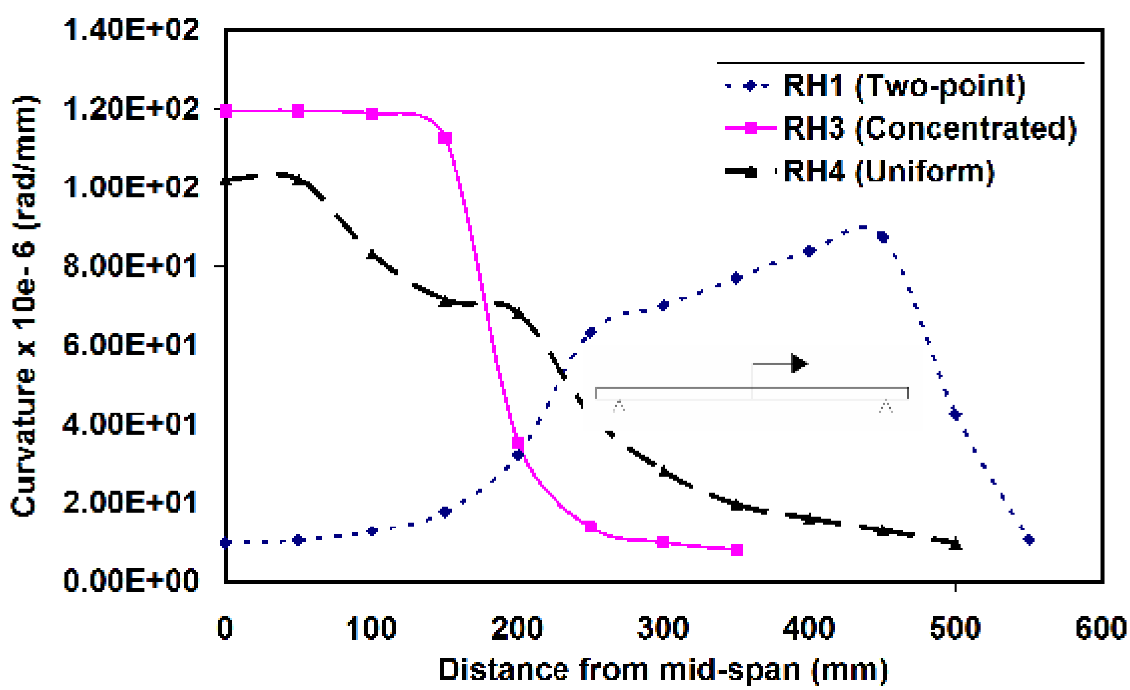


Fig. 22. Distribution of curvature in RH1, RH3 and RH4 beams

The variation of $q_p$ and $l_p$ for the different loading types in beams, could be explained by the differences in the bending moment diagrams and yielding lengths ($l_y$) for each type of loading which has been shown in Fig. 22. This may be due to moment gradient in neighborhood of the critical section. i.e., bending moment distribution has significant influence on the distribution of curvature along the length of the beam. Variation of $q_p$ with respect to $r$ in the different loading types is presented in Fig. 23. As could be seen in this figure, plastic hinge rotation of 2-point loaded beam is greater than that in uniform case and subsequently the $q_p$ of uniform loaded beam is greater than the concentrate loaded beam in the whole different ratios of tensile reinforcements.

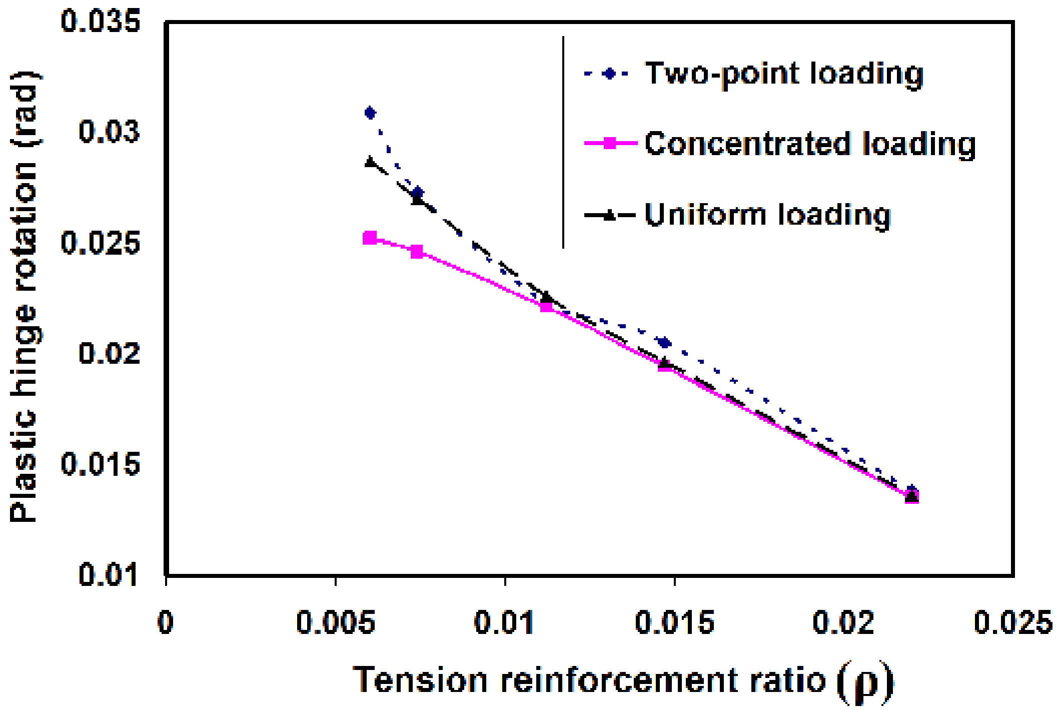


Fig. 23. Variation of $q_p$ with respect to $r$ in different loading types

### e.4. Empirical and proposed equations

The most widely used $l_p$ formulations for RC beams and columns available in literature are presented in Table 13. Where, z = distance from critical section to point of contraflexure, d = effective depth of section, $d_b$ = diameter of longitudinal reinforcement, L = length of the member, h = overall depth of section, $f_y$ = yielding stress of reinforcement and $f_c'$ = concrete compressive strength.

As it shown in this table and previous results, the most part of these obtained empirical values are close to RHPFRCC beams under concentrated loading which is changed from 170 to 215 mm. The values of $l_p$ for uniform and two-point loaded beams vary from 220 to 245 and 256 to 298 mm respectively. These analytical values are close to results which have been presented by Sheikh and Khoury, Bayrak and Sheikh, Panagiotakos and Fardis.

Table 13. Plastic hinge length formulations

| Researcher(s) | Element Type | Plastic hinge length expression ($l_p$) | Present beam using empirical equations $l_p$ (mm) |
|---|---|---|---|
| Baker (1956) | RC beams and columns | $k \cdot \left( z/d \right)^{1/4} \cdot d$ | 189.6 |
| I.C.E (1962) | RC beams and columns | $k_1 k_2 k_3 \cdot \left( z/d \right)^{1/4} \cdot d$ | 189 |
| Sawyer (1964) | | $0.25d + 0.075z$ | 146.25 |
| Corley (1966) | RC beams | $0.5d + z/\sqrt{d}$ | 199 |
| Mattock (1967) | RC beams | $0.5d + 0.05z$ | 187.5 |
| Park et al (1982) | RC columns | $0.42h$ | 126 |
| Mander (1983) | RC columns | $0.32\sqrt{d_b} + 0.06L$ | 139.28 |
| Priestley and Park (1987) | RC columns | $0.88d_b + 0.08z$ | 98.08 |
| Sakai and Sheikh (1989) | RC beams and columns | $0.35h \sim 0.7h$ | 105 ~210 |
| Tanaka and Park (1990) | RC columns | $0.4h \sim 0.75h$ | 120~225 |
| Paulay and Priestley (1992) | RC beams and columns | $0.022d_b f_y + 0.08z$ | 224.8 |
| Sheikh and Khoury (1993) | RC columns | $0.95h \sim 1.15h$ | 285~345 |

| | | | |
|---|---|---|---|
| Watson and Park (1994) | RC columns | $0.56h$ | 168 |
| Bayrak and Sheikh (1997) | RC columns | $1h$ | 300 |
| Panagiotakos and Fardis (2001) | RC beams and columns | $0.021 d_b f_y + 0.18z$ | 323.4 |
| Berry et al (2008) | RC columns | $0.05L + 0.1\frac{f_y d_b}{\sqrt{f_c'}}$ | 156.3 |

Naaman et al (Naaman et al 1996), presented a simple formulation for calculating $l_y$ in reinforced HPFRCC beams which is presented in Eq. (6).

$$l_y = (1.06 + 0.13 r V_f) \cdot d$$

Eq. (6)

Where, $r$ is the tensile reinforcement ratio in percent, $V_f$ is the volume fraction fibers in percent and $d$ is the effective depth of beam. For the present study $l_y$ is equal to 364.82 mm which is close to obtained values in Table 10.

The relation among three different types of loading discussed in this paper can be defined as:

$$a_{u(Two-point)} = \frac{q_{P\ (Two-point.)}}{q_{P\ (Conc.)}}$$

$$a_{u(Uni)} = \frac{q_{P\ (Uni.)}}{q_{P\ (Conc.)}}$$

Eq. (7)

Where, $a_u$ is the loading type factor.

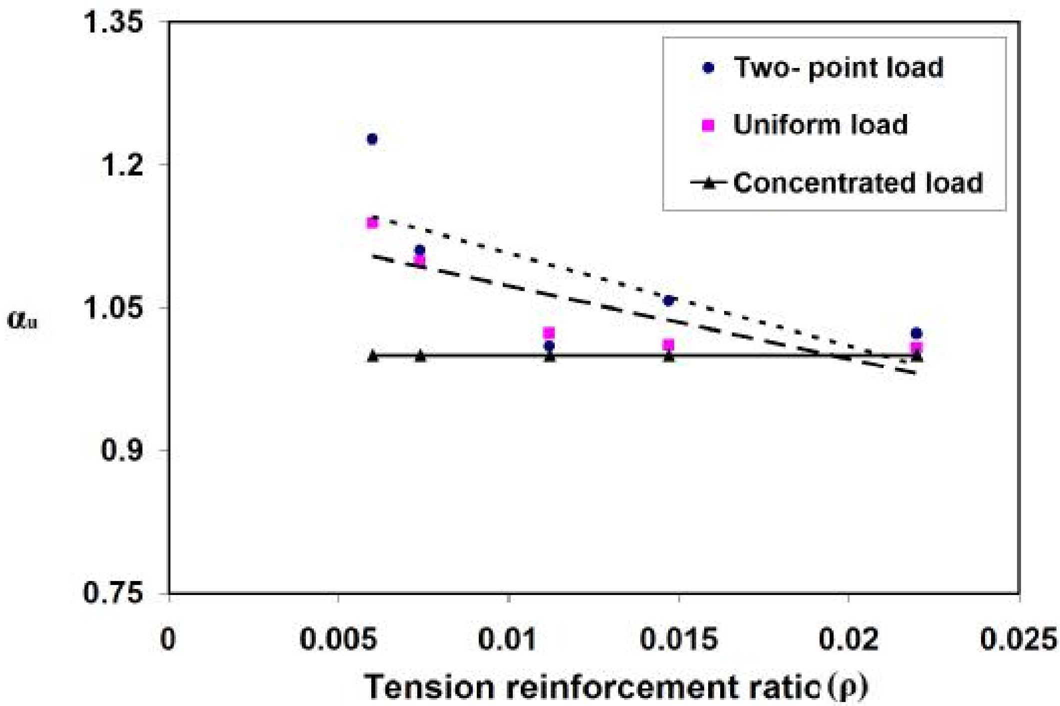


Fig. 23. Relation among three different types of loading

The variation of $a_u$ with tension reinforcement ratio is presented in Fig. 24. Regression analysis of the results can be expressed as:

$$a_{u(Two-po\,\mathrm{int})} = 1.2\ (1 - 8.1r)$$

$$a_{u(Uni)} = 1.15\ (1 - 6.7r)$$

Eq. (8)

The analytical values of the plastic hinge rotation and the estimated values using equation 8 are compared to each other in Table 14.

Table 14. Analytical and estimated values for $q_p$

| Name of model | $a_u$ | $q_{P\ (Analytical)}$ (rad) | $q_{P\ (Estimated)}$ (rad) | $\frac{q_{P\ (Estimated)}}{q_{P\ (Analytical)}}$ |
|---|---|---|---|---|
| RH1 | 1.091 | 0.0223 | 0.0241 | 1.08 |
| RH5 | 1.142 | 0.0309 | 0.0288 | 0.93 |
| RH6 | 1.128 | 0.0273 | 0.0278 | 1.02 |
| RH7 | 1.057 | 0.0205 | 0.0205 | 1 |
| RH8 | 0.986 | 0.0138 | 0.0133 | 0.96 |
| RH4 | 1.064 | 0.0226 | 0.0235 | 1.04 |
| RH13 | 1.104 | 0.0287 | 0.0278 | 0.97 |
| RH14 | 1.093 | 0.027 | 0.0269 | 0.99 |
| RH15 | 1.037 | 0.0197 | 0.0201 | 1.02 |
| RH16 | 0.98 | 0.0136 | 0.0132 | 0.97 |

The maximum difference among analytical and estimated values is about 8 %. It can be noted that in two-point loaded beam, the distance between two concentrated loads are significant and has an influence on previous results(Harajli and Hijazi 1991).

## f. Conclusions

Based on the analytical and experimental results, the following conclusions can be drawn:

1. The yield and ultimate loads increase with the tension reinforcement ratio ( $r$ ) in RHPFRCC beams, but the ultimate deflection, ultimate curvature and ductility ratio decrease.

2. The value of plastic hinge length and plastic hinge rotation of RHPFRCC simply supported beams are more 1.065 and 1.77 times more than similar RC beams.

3. The plastic hinge length and rotation increase as the loading type changed from concentrated load to uniform load and two-point load. But in the case of two-point load, the results are independent to the distance between two loads.

4. In the case of two-point loading, the plastic hinge length and rotation of RHPFRCC beams are about 1.05 and 1.8 times more than RC beams. But the yield length in both beams is the same approximately. Plastic hinge length and rotation of RHPFRCC concentrate loaded beams are about 0.72 and 1.65 times compared to RC beams under two-point loading. And in uniform loaded beams, these values are 0.86 and 1.76 respectively.

5. The yielding length of two-point loaded HPFRCC beam is longer than other beams. The ultimate curvature of concentrate loaded beam is greater than others. The area under the curve of two-point loaded HPFRCC beam is more than other beams and concluded to more $q_p$ and $l_p$ values.

6. Empirical equations for calculating $l_p$ could be used for determining the plastic hinge length of RHPFRCC beams under concentrated loading. For other types of loading the

equations which have been presented by Sheikh and Khoury, Bayrak and Sheikh, Panagiotakos and Fardis and Naaman et al can be used.

7. The analytical results indicate that the proposed equations for different loading types and tension reinforcement ratios are adequate and the difference between analytical and estimated values of $q_P$ is about 8 % in the maximum case.

## References


Baker, A.L.L. (1956). "Ultimate load theory applied to design of reinforced and prestressed concrete frames", Concrete Publications, London.

Bayrak, O. and Sheikh, S.A. (1997). "High strength concrete columns under simulated earthquake loading", ACI Structural Journal, **94**(6), 708-722.

Berry, M., Lehman, D.E., and Lowes, L.N. (2008). "Lumped plasticity models for performance simulation of bridge columns", ACI Structural Journal, **105**(3), 270-279.

Corley, W.G. (1966). "Rotational capacity of reinforced concrete beams", Journal of Structural Division, ASCE, **92**, 121-146.

Fischer, G. and Li, V.C. (2000). "Structural composites with ECC," Proceedings of the ASCCS-6, Ed. Y. Xiao and S.A. Mahin, USC, pp. 1001-1008.

Fischer, G., Wang, S. and Li, V.C. (2003). "Design of engineered cementitious composites for processing and workability requirements", Seventh International Symposium on Brittle Matrix Composites, pp. 29-36. Warsaw, Poland.

Fukuyama, H., Matsuzaki, Y., Sato, Y. and Iso, M. (2000). "Structural performance of engineered cementitious composite elements".

Ghobarah, A. and Aly, N.M. (1998). "Seismic reliability assessment of existing reinforced concrete buildings", Journal of Earthquake engineering, **2**(4), 569-592.

Han, T.S. and Feenstra, P.H. and Billington, S.L. (2003). "Simulation of highly ductile fiber-reinforced cement-based composite components under cyclic loading", ACI Structural Journal, **100**(6), 749-757.

Hung, C.C and El-Tawil, S. (2010). " Hybrid rotating/fixed-crack model for high performance fiber reinforced cementitious composites” ACI Materials J., 568-576.

I.C.E. Research Committee. (1962). "Ultimate load design of concrete structures", **21**, 399-442.

Kabele, P. and Horii, H. (1996). “Analytical model for fracture behaviors of pseudo strain-hardening cementitious composites" Journal of Materials, Concrete Structures and Pavements, 30(532), 208-219.

Kheyroddin, A. (1996). "Nonlinear finite element analysis of flexure-dominant reinforced concrete structures", PhD Thesis, McGill University, 290.

Kheyroddin, A. and Naderpour, H. (2007). "Plastic hinge rotation capacity of reinforced concrete beams", International Journal of Civil Engineering, 5(1), 30-47.

Kong, H.J., Bike, S. and Li, V.C. (2003). "Development of a self-compacting engineered cementitious composite employing electrosteric dispersion/stabilization", Journal of Cement and Concrete Composites 25(3), 301-309.

Harajili, H. and Hijazi, S. (1991). "Evaluation of the ultimate steel stress in partially prestressed concrete members", PCI Journal, 62-82.

Help of ABAQUS. (2008). "Getting started with ABAQUS".

Lee, B.Y., Kim, J.K. and Kim Y.Y. (2010), “Prediction of ECC tensile stress-strain curves based on modified fiber bridging relations considering fiber distribution characteristics”. Computers and Concrete, An Int'l Journal, 7(5).

Lepech, M.D., Li, V.C., Robertson, R.E. and Keoleian, G.A. (2007). "Design of ductile engineered cementitious composites for improved sustainability", ACI Materials Journal.

Li, V.C. and Wu, H.C. (1992), "Conditions for pseudo strain-hardening in fiber reinforced brittle matrix composites", J. Applied Mechanics Review, 45(8), 390-398.

Li, V.C. (2007). "Engineered cementitious composites (ECC) – material, structural, and durability performance", University of Michigan, Ann Arbor, MI 48109.

Mander, J.B. (1983). "Seismic design of bridge piers", PhD Thesis, University of Canterbury.

Mattock, A.H. (1967). "Discussion of rotational capacity hinging regions in reinforced concrete beams", Journal of Structural Division, ASCE, **93**, 519-522.

Na, C. and Kwak, H.G. (2011). “A numerical tension stiffening model for ultra high strength fiber reinforced concrete beams”. Computers and Concrete, An Int'l Journal, 8(1).

Naaman, A.E. and Reinhardt, H.W. (1996). "Characterization of high performance fiber reinforced cement composites", HPFRCC-2, 1-24.

Naaman, A.E., Paramasivam, P., Balazs, G., Bayasi, Z.M., Eibl, J., Erdelyi, L., Hassoun, N.M., Krstulovic, N., Li, V.C. and Lohrmann, G. (1996). "Reinforced and prestressed concrete using HPFRCC materials", HPFRCC-2, 314-320.

Panagiotakos, T.B. and Fardis, M.N. (2001). "Deformation of reinforced concrete members at yielding and ultimate, haracterization of high performance fiber reinforced cement composites", ACI Structural Journal, **98**(2), 135-148.

Park, R., Priestley, M.J.N. and Gill, W.D. (1982). "Ductility of square confined concrete columns", Structural Journal, **108**(ST4), 929-950.

Paulay, T. and Priestley, M.J.N. (1992). "Seismic design of reinforced concrete and masonry structures", John Wiley & Sons.

Priestley, M.J.N. and Park, R. (1987). "Strength and ductility of concrete bridge columns under seismic loading", ACI Structural Journal, **84**(1), 61-76.

Ranzi, G. and Bradford, M.A. (2009). "Nonlinear analysis of composite beams with partial shear interaction by means of the direct stiffness method", Steel and Composite Structures, 9(2).

Sakai, K. and Sheikh, S.A. (1989). "What do we know about confinement in reinforced concrete columns", ACI Structural Journal, **86**(2), 192-207.

Shaheen, E. and Shrive, N.G. (2008). "Cyclic loading and fracture mechanics of Ductal concrete", International Journal of Fracture, **148**(3), 251-260.

Shayanfar, M.A., Kheyroddin, A. and Mirza, M.S. (1996). "Element size effects in nonlinear analysis of reinforced concrete members", Computers & Structures, London, U.K.

Sheikh, S.A. and Khoury, S.S. (1993). "Confined concrete columns with stubs", ACI Structural Journal, **90**(4), 414-431.

Sirijaroonchai, K. (2009). "A macro-scale plasticity model for high performance fiber reinforced cement composites", PhD Dissertation, Michigan University.

Suwannakarn, S.W. (2009). "Post-cracking characteristics of high performance fiber reinforced cementitious composites", PhD Dissertation, Michigan University.

Tanaka, H. and Park, R. (1990). "Effect of lateral Confining reinforcement on the ductile behavior of reinforced concrete columns", Research Report, University of Canter bury.

Wang, S. and Li, V.C. (2003). "Materials design of lightweight PVA-ECC". In Proc., HPFRCC, A.E. Naaman and H.W. Reinhardt, eds., pp.379-390.

Wang, S. and Li, V.C. (2006). "High early strength engineered cementitious composites", ACI Materials Journal, **103**(2), 97-105.

Watson, S. and Park, R. (1994). "Simulated seismic load tests on reinforced concrete columns", Journal of Structural Engineering, **120**(6), 1825-1849.